Measurement of the cross sections of the ^{25}Mg$(n, \alpha)^{22}$Ne reaction in the 4–6 MeV region

Yu. M. Gledenov and M. V. Sedysheva
Frank Laboratory of Neutron Physics, JINR, Dubna 141980, Russia

G. Khuukhenkhuu
Nuclear Research Centre, National University of Mongolia, Ulaanbaatar, Mongolia

Huaiyong Bai, Haoyu Jiang, Yi Lu, Zengqi Cui, Jinxiang Chen, and Guohui Zhang*
State Key Laboratory of Nuclear Physics and Technology, Institute of Heavy Ion Physics, Peking University, Beijing 100871, China

(Received 22 June 2018; published 10 September 2018)

Cross sections of the ^{25}Mg$(n, \alpha)^{22}$Ne and the ^{25}Mg$(n, \alpha_0)^{22}$Ne reactions were measured at five neutron energy points in the 4.0–6.0 MeV region. Highly enriched (98.6%) ^{25}MgO samples were prepared. A twin-gridded ionization chamber was used as the charged particle detector and the ^{238}U(n, f) reaction was utilized to calibrate the absolute neutron fluence. The present results were compared with those of the existing measurements, evaluations, and calculations.

DOI: 10.1103/PhysRevC.98.034605

I. INTRODUCTION

Most of the neon in meteoroids is generated from the irradiation of the magnesium by the cosmic ray, and the content of neon can more or less indicate the exposure time of the meteoroids [1]. The secondary particles induced by neutrons with energy below 100 MeV play a crucial role in the isotope production [2]. However, the cross section data of neon production from magnesium irradiated by neutrons are scarce [1].

Among the magnesium isotopes, the abundance of ^{25}Mg is 10% [3]. So, cross sections of the ^{25}Mg$(n, \alpha)^{22}$Ne reaction (Q value: 0.48 MeV) are important but the related measurements are scanty. Up to date, only two data points in the MeV region measured by Lavielle [2] are included in the EXFOR library [4], and the discrepancies among different evaluations are apparent [5]. Furthermore, no evaluation goes through both the two data points. So, new measurements are demanded to constrain the corresponding excitation function.

In the present work, cross sections of the ^{25}Mg$(n, \alpha)^{22}$Ne and the ^{25}Mg$(n, \alpha_0)^{22}$Ne reactions were measured at five energy points in the 4–6 MeV region with step of 0.5 MeV. Details of the experiments are introduced in Sec. II. The data processing and the results are illustrated in Sec. III. The conclusions are drawn in Sec. IV.

II. DETAILS OF THE EXPERIMENTS

A. Experimental setup

The sketch of the experimental setup, which consists of a neutron source, a twin-gridded ionization chamber, and a BF_3 long counter, is illustrated in Fig. 1. The neutrons were generated using deuteron beam to bombard a deuterium gas target 2.0 cm in length and 0.30 MPa in pressure. The deuteron beam ($\sim$2.5 μA) was accelerated by the 4.5 MV Van de Graff accelerator of Peking University. The deuterium gas target was separated from the vacuum tube of the accelerator by a molybdenum membrane 5.0 μm in thickness. The gas target was cooled by a compressed air jet. In the present work, the neutron energy resolution ranged from 0.1–0.2 MeV.

A twin-gridded ionization chamber was used as the charged particle detector as shown in Fig. 1. The cathode-grid and the anode-grid distances were 6.1 and 1.5 cm, respectively. The working gas (Kr + 2.7% CO_2) pressures of the ionization chamber were 0.052 MPa for 4.0–5.0 MeV region and 0.068 MPa for 5.5–6.0 MeV region, respectively. The cathode of the ionization chamber contained a sample changer with five sample positions [6]. Back-to-back samples can be mounted at each of them. At three of the five sample positions, back-to-back four-peaks α-sources [7], back-to-back ^{25}MgO samples (details of which are presented in Table I), and back-to-back Ta backings were mounted, separately. At the fourth sample position, a circular ^{238}U standard sample (enrichment > 99.999%) with radius 22.5 mm was mounted to calibrate the absolute neutron fluence. The number of the ^{238}U nuclei N_U was 2.064×10^{19} ($\pm$0.45%) measured utilizing its α activity [8]. The samples can be replaced through rotating the knob below the ionization chamber without opening it [6]. Apart from the measured samples, the other samples were shielded by aluminum plates of the cathode in both the forward (0°–90°) and the backward (90°–180°) directions with respect to the deuteron beam axis [9]. The charged particles emitted from the measured samples in both the forward and the backward directions can be measured. The measured samples were at 0° with respect to the deuteron beam axis departing from the center of the deuterium gas target by 16.5 cm. The cathode-anode two-

*Corresponding author: guohuizhang@pku.edu.cn

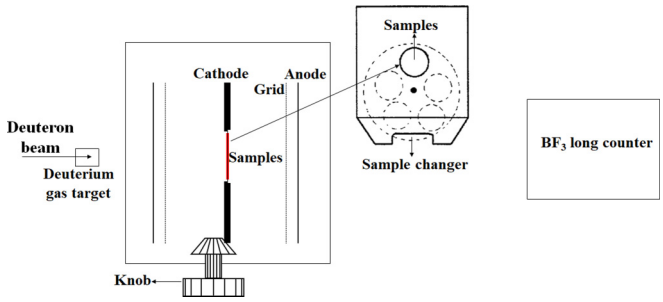

FIG. 1. Sketch of the experimental setup.

dimensional spectra of the cathode-anode coincidence signals in the forward and the backward directions were separately recorded. The data acquisition system (DAqS) was introduced in Ref. [10].

A BF_3 long counter, details of which were presented in Ref. [11], located at 0° with respect to the deuteron beam axis, was used to monitor the relative neutron fluence. The outer radius of the BF_3 long counter was 27 mm and the length of it was 300 mm. The BF_3 long counter was surrounded by a moderator with radius of 350 mm and length of 400 mm, and a cadmium plate 0.5 mm in thickness was mounted at the front face of the counter. The distance between the front face of the BF_3 long counter and the center of the gas target was about 3.0 m.

B. Process of the measurements

The experiments were conducted at five neutron energy points in 4.0–6.0 MeV region. At each energy point, five runs of measurements were executed. First, the experimental setup was calibrated using the four-peaks α-sources. Second, the back-to-back ^{25}MgO samples were measured (foreground). Third, the back-to-back Ta backings were measured (background). Fourth, the $^{238}U(n, f)$ events were detected to calibrate the absolute neutron fluence. Finally, the experimental setup was calibrated again to check the stability of it. The relative neutron fluence was monitored by the BF_3 long counter for all runs apart from the two runs of calibrations. The beam duration ranged from 10–16 h for each energy point and the total beam duration was about 65 h.

III. DATA PROCESSING AND THE RESULTS

After the measurements, the data were processed in six steps. First, the calibration of the experimental setup was executed to decide the effective area of the α events and to determine the corresponding energy of each anode channel. Second, the background was deducted to obtain the net α events emitted from the ^{25}MgO samples. Third and fourth, the simulation of the α events emitted from the $O(n, \alpha)C$ and $^{25}Mg(n, \alpha)^{22}Ne$ reactions were performed to decide the measurement threshold and the detection efficiency, separately. Fifth, the calibration of the neutron fluence using $^{238}U(n, f)$ reaction was processed. Finally, the corresponding cross sections were determined.

A. Calibration of the experimental setup

The calibration using the four-peaks α sources determined not only the effective area of the α events in the cathode-anode two-dimensional spectra, but also the corresponding energy of each anode channel. Examples of the calibration results are shown in Figs. 2 and 3. The cathode-anode two-dimensional spectra measured in the forward and the backward directions are shown in Fig. 2. The areas between the two dashed curves in Fig. 2 are the effective areas of the α events emitted from the $^{25}Mg(n, \alpha)^{22}Ne$ reaction. Considering the energy resolution of the experimental setup, the area between the two dashed curves is wider than that between the 0° curve and the 90° line as shown in Fig. 2. The relationships between the anode channel numbers and the corresponding energies are presented in Fig. 3.

B. Background deduction

To obtain the α events emitted from the $^{25}Mg(n, \alpha)^{22}Ne$ reaction, the backgrounds must be deducted from the foregrounds in both the forward and the backward directions. The relative neutron fluence monitored by the BF_3 long counter was used for normalization. Examples of the results after backgrounds deduction are illustrated in Fig. 4. The events within the effective areas (between the two dashed curves in Fig. 4) were projected to get the anode spectra as shown in Fig. 5.

C. Interferences of the events emitted from the O(n, α)C reaction

In Fig. 5, the net event was obtained using the counts from the measurement of the ^{25}MgO samples (foreground) deducting that from the measurement of the Ta backings (background), i.e., the α events generated through the $^{25}Mg(n, \alpha)^{22}Ne$ and the $O(n, \alpha)C$ reactions. Thus the measurement threshold must be carefully chosen to exclude the interferences of the α events emitted from the $O(n, \alpha)C$ reaction. To do this, the anode spectra of the α events emitted from the $O(n, \alpha)C$ reaction should be decided first. In the present work, the O was assumed only consisted of ^{16}O, which will not bring noticeable deviations because the abundance of ^{16}O was as high as 99.8% [3] and the (n, α) reaction cross sections for ^{17}O (abundance $< 0.1\%$) and ^{18}O (abundance $\approx 0.2\%$) were not big in this neutron energy region. The angular differential cross sections of the $^{16}O(n, \alpha)^{13}C$ reaction with

TABLE I. Details of the ^{25}MgO samples.

Direction	Enrichment	Radius (mm)	^{25}Mg nucleus number	Backing
Forward	98.6%	22.0	1.623×10^{20} (±5%)	Ta plate 0.1 mm in thickness
Backward	98.6%	22.0	1.580×10^{20} (±5%)	Ta plate 0.1 mm in thickness

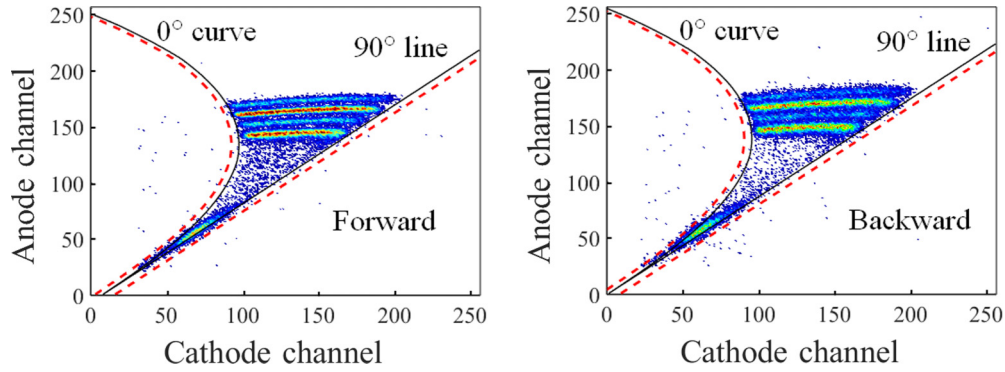

FIG. 2. The cathode-anode two-dimensional spectra of the four-peaks α sources in the forward (left) and the backward (right) directions.

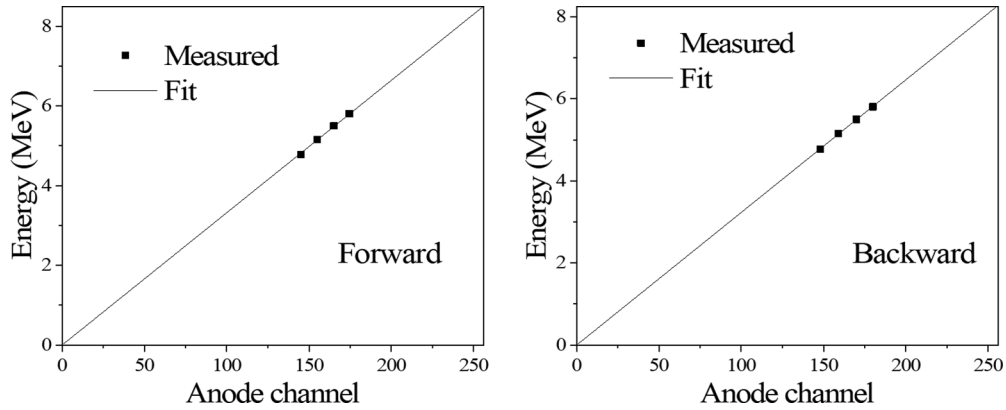

FIG. 3. The relationships between the anode channel numbers and the corresponding energies in the forward (left) and the backward (right) directions.

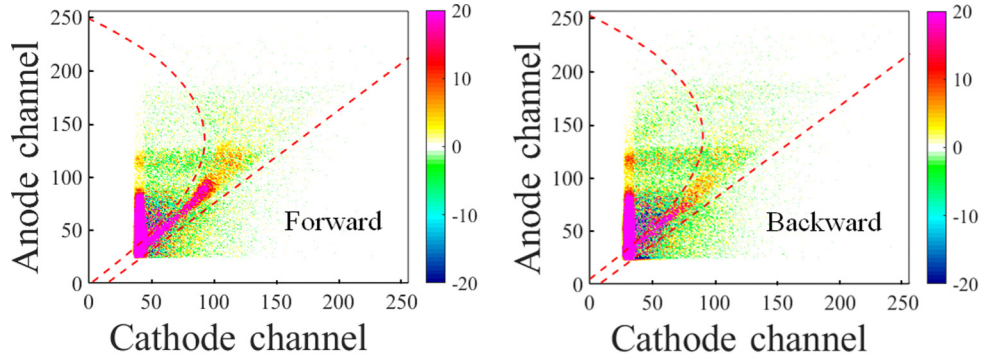

FIG. 4. The cathode-anode two-dimensional spectra after the background deduction in the forward (left) and the backward (right) directions for the measurement at $E_n = 4.0\,\mathrm{MeV}$.

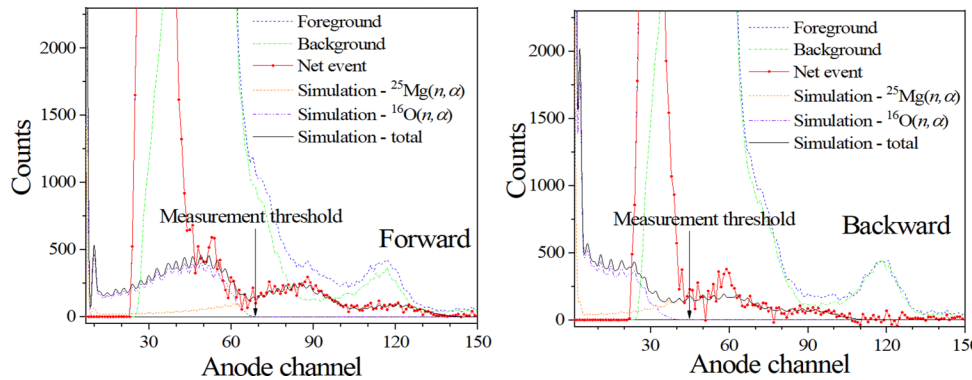

FIG. 5. The anode spectra of the events in the forward (left) and the backward (right) directions for the measurement at $E_n = 4.0\,\mathrm{MeV}$.

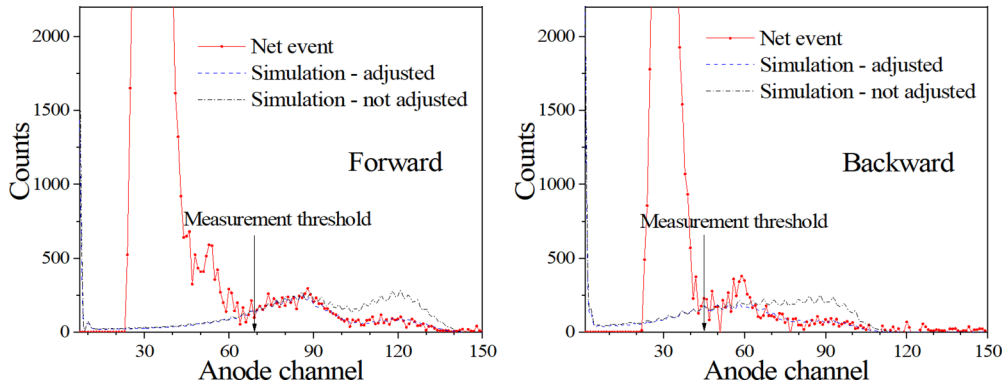

FIG. 6. The anode spectra of the events in the forward (left) and the backward (right) directions for the measurement at $E_n = 4.0$ MeV. The dotted line is the measured one. The dashed line and the dash-dotted line are the simulated ones with and without adjusting the cross section of the ^{25}Mg$(n, \alpha_0)^{22}$Ne reaction ($\times 0.30$), separately.

the residual ^{13}C in different excited states were calculated using TALYS-1.8 code [12]. Then, the anode spectra of the α events emitted from the ^{16}O$(n, \alpha)^{13}$C reaction were simulated with Monte Carlo method in which the wall effect of the sample position well [9] was considered.

The Monte Carlo simulation was similar to that described in Ref. [9]. In the simulation, the α events emitted from the ^{16}O$(n, \alpha)^{13}$C reaction with the residual ^{13}C in different excited states were processed one by one. Besides the angular differential cross sections of the ^{16}O$(n, \alpha)^{13}$C reaction calculated by TALYS-1.8 code [12], the stopping powers calculated by SRIM-2013 code [13] were also utilized. It should be pointed out that the counts of the simulated anode spectra may be higher or lower than the measurements because the calculated cross section of the ^{16}O$(n, \alpha)^{13}$C reaction may be inaccurate, so each of the simulated anode spectra was multiplied by a factor to fit the measurements. Examples of the simulated results are presented in Fig. 5 as "Simulation - ^{16}O(n, α)". Although the working gas contains ^{16}O, it was not considered here because the related interferences can be deducted in background deduction.

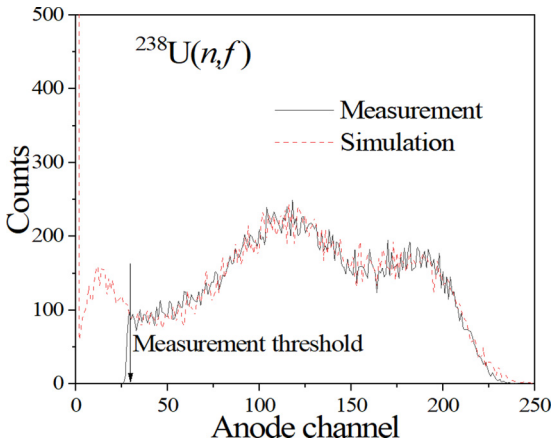

FIG. 7. The anode spectra of the fission fragments. The solid line is the measured one and the dashed line is the simulated one.

D. Detection efficiency of the events emitted from the ^{25}Mg$(n, \alpha)^{22}$Ne reaction

Because not all the α events emitted from the ^{25}Mg$(n, \alpha)^{22}$Ne reaction can be detected, the detection efficiency must be decided to calculate the total number of the α events. With the simulated anode spectra of the α events emitted from the ^{16}O$(n, \alpha)^{13}$C reaction, the measurement threshold, which was higher than the region of the α events emitted from the ^{16}O$(n, \alpha)^{13}$C reaction to exclude their interferences, was decided as shown in Fig. 5. In addition, because the enrichment of ^{25}Mg was 98.6%, the enrichment of ^{24}Mg was about 1.4%. Since the Q value of the ^{16}O$(n, \alpha)^{13}$C reaction (–2.21 MeV) was higher than that of the ^{24}Mg$(n, \alpha)^{21}$Ne reaction (-2.55 MeV), the interferences of the ^{24}Mg$(n, \alpha)^{21}$Ne reaction were also excluded by the measurement threshold.

Being similar to the simulation of the α events emitted from the ^{16}O$(n, \alpha)^{13}$C reaction, the anode spectra of the α events emitted from the ^{25}Mg$(n, \alpha)^{22}$Ne reaction were also

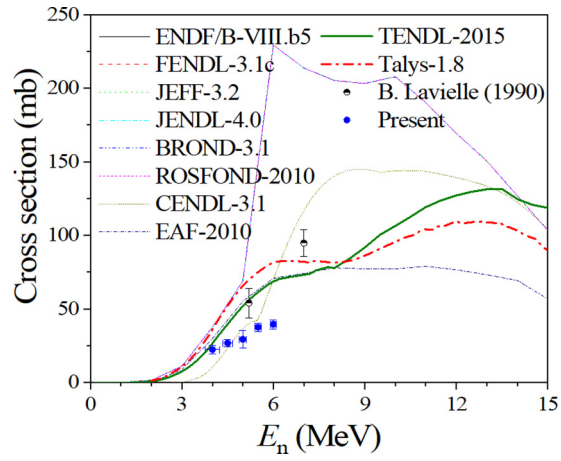

FIG. 8. Present cross sections of the ^{25}Mg$(n, \alpha)^{22}$Ne reaction compared with existing measurements, evaluations and TALYS-1.8 code calculations. The data of Lavielle is taken from Ref. [2], and the evaluations are taken from ENDF library [5].

simulated using the Monte Carlo simulations. Examples of the simulated results are shown in Fig. 5 as "Simulation - ^{25}Mg(n,α)". It should be pointed out that, in the simulation, the calculated cross section of the ^{25}Mg$(n,\alpha_0)^{22}$Ne reaction was multiplied by a factor to match the measurement. As examples, the differences with and without adjusting the cross section of the ^{25}Mg$(n,\alpha_0)^{22}$Ne reaction are shown in Fig. 6. With the simulated anode spectra of the α events emitted from the ^{25}Mg$(n,\alpha)^{22}$Ne reaction, the detection efficiency ε_α (58%–73%) of the α events above the measurement threshold can be decided. So, the total number of the α events N_α can be obtained as $N_{d\alpha}/\varepsilon_\alpha$ where the $N_{d\alpha}$ was the detected number of the α events above the measurement threshold.

E. Neutron fluence calibration using the ^{238}U(n, f) reaction

In the present work, a ^{238}U sample was used to calibrate the neutron fluence. The neutron fluence N_{fluf} during the measurement of the ^{238}U(n, f) reaction can be decided as

$$N_{fluf} = \frac{N_{df}}{\sigma_f N_U \varepsilon_f}, \tag{1}$$

where N_{df} is the detected fission events, σ_f is the cross section of the ^{238}U(n, f) reaction taken from the Neutron Cross-section Standards [14], N_U is the ^{238}U nucleus number, and ε_f is the detection efficiency.

In the present work, the detection efficient ε_f was obtained using Monte Carlo simulation details of which can be seen in Ref. [8]. In the simulation, the fission products yields taken from ENDF/B-VII.1 library [15], the energies of the fission fragments as a function of their masses published by Birgersson [16], and the stopping powers calculated using SRIM-2013 code [13] were used. The measured and simulated anode spectra of the fission fragments are shown in Fig. 7. Then, the detection efficiency ε_f (about 80%) above the measurement threshold can be determined. So, the neutron fluence through the ^{238}U sample N_{fluf} can be decided using Eq. (1). With the counts of the BF_3 long counter during the measurement of the ^{25}MgO samples $N_{B\alpha}$ and that of the ^{238}U sample N_{Bf}, the neutron fluence through the ^{25}MgO samples $N_{flu\alpha}$ during the measurement of the ^{25}MgO samples can be decided as

$$N_{flu\alpha} = N_{fluf}\frac{N_{B\alpha}}{N_{Bf}}. \tag{2}$$

TABLE II. The measured cross sections of the ^{25}Mg$(n,\alpha)^{22}$Ne and the ^{25}Mg$(n,\alpha_0)^{22}$Ne reactions.

E_n (MeV)	^{25}Mg$(n,\alpha)^{22}$Ne (mb)	^{25}Mg$(n,\alpha_0)^{22}$Ne (mb)
4.0 ± 0.2	22.32 ± 3.03	5.82 ± 0.86
4.5 ± 0.2	26.71 ± 2.62	9.37 ± 1.06
5.0 ± 0.1	29.31 ± 6.09	12.35 ± 2.19
5.5 ± 0.1	37.47 ± 2.79	10.53 ± 0.75
6.0 ± 0.1	39.46 ± 3.18	13.78 ± 1.24

F. Calculation of the cross sections and the results

With the number of the ^{25}Mg nuclei N_{Mg}, the total counts of the α events N_α and the neutron fluence through the ^{25}MgO samples $N_{flu\alpha}$ in Eq. (2), the cross section of the ^{25}Mg$(n,\alpha)^{22}$Ne reaction σ_α can be decided as

$$\sigma_\alpha = \frac{N_U N_{Bf} N_{d\alpha} \varepsilon_f}{N_{Mg} N_{B\alpha} N_{df} \varepsilon_\alpha}\sigma_f. \tag{3}$$

The present cross sections are illustrated in Fig. 8 and Table II, and the uncertainty analysis of the measurement is presented in Table III.

As shown in Fig. 8, apart from the present results, only two data points measured by Lavielle [2], which was conducted through measuring the production of ^{22}Ne using a mass spectrometer, are included in the EXFOR library [4]. However, no evaluation goes through both of these two data points. The present cross sections are much lower than the only existing results. The tendency of the present results is different from all the evaluations, and except for CENDL-3.1, all the evaluations and the calculation (calculated by TALYS-1.8 code [12] with default input parameters) are higher than the present measurements. Since the related data are scarce, to obtain a reliable ^{25}Mg$(n,\alpha)^{22}$Ne excitation function, more measurements and improved evaluations are demanded.

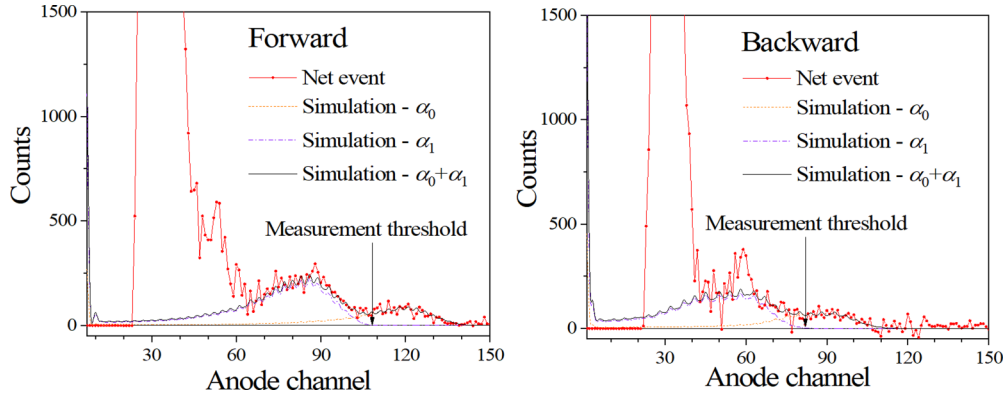

FIG. 9. The anode spectra of the events in the forward (left) and the backward (right) directions for the measurement at $E_n = 4.0$ MeV. The dotted line is the measured one, the dashed line and the dash-dotted line are the simulated results of the ^{25}Mg$(n,\alpha_0)^{22}$Ne and the ^{25}Mg$(n,\alpha_1)^{22}$Ne reactions, separately, and the solid line is the summation of the dashed line and the dash-dotted line.

TABLE III. The sources of the uncertainty.

Sources of the uncertainty	Magnitude (%)	
	^{25}Mg$(n,\alpha)^{22}$Ne	^{25}Mg$(n,\alpha_0)^{22}$Ne
N_U, the number of the ^{238}U nuclei.	0.5	
N_{Mg}, the number of the ^{25}Mg nuclei.	3.5–3.6	
$N_{Bf}/N_{B\alpha}$, the ratio of the count of the BF_3 long counter during the measurement of the ^{238}U sample over that during the measurement of the ^{25}MgO samples.	2.3–5.8	
$N_{d\alpha}$, the detected counts of the α events.	5.9–12.9	5.5–9.5
N_{df}, the detected fission events.	0.5–0.6	
ε_f, the detection efficiency of the fission events.	1.0–1.1	
ε_α, the detection efficiency of the α events.	0.5–14.7	
σ_f, the cross section of the ^{238}U(n,f) reaction.	0.7–0.9	
Total	7.4–20.8	7.1–17.8

With the similar processing method to determine the cross section of the ^{25}Mg$(n,\alpha)^{22}$Ne reaction, the cross section of the ^{25}Mg$(n,\alpha_0)^{22}$Ne reaction can be obtained by setting a measurement threshold, which can exclude the interferences of the ^{25}Mg$(n,\alpha_1)^{22}$Ne reaction as illustrated in Fig. 9. The obtained cross sections of the ^{25}Mg$(n,\alpha_0)^{22}$Ne reaction are illustrated in Fig. 10 and Table II, and the uncertainty is presented in Table III. In Fig. 10, the data of Ashery [17] and Wolke [18] are characterized by "Detailed balance" because the original measured cross sections are those of the ^{22}Ne$(\alpha,n_0)^{25}$Mg reaction. Using the detailed balance principle [19], the cross sections are transformed into those of the ^{25}Mg$(n,\alpha_0)^{22}$Ne reaction.

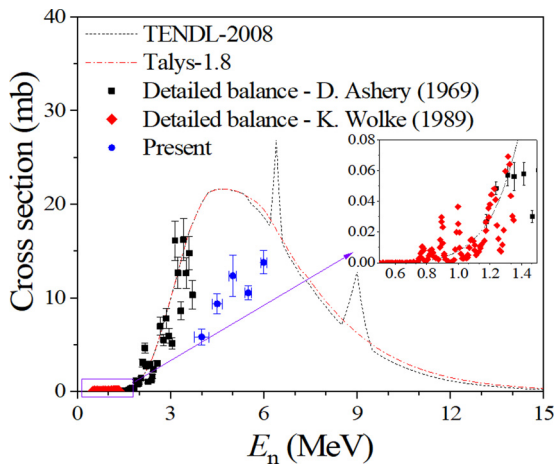

FIG. 10. Present cross sections of the ^{25}Mg$(n,\alpha_0)^{22}$Ne reaction compared with existing measurements, evaluations and TALYS-1.8 code calculations. The data of Ashery and Wolke are taken from Refs. [17,18]. Because the original cross sections in Refs. [17,18] are those of the ^{22}Ne$(\alpha,n_0)^{25}$Mg reaction, the results, which are calculated according to the detailed balance principle, are characterized by "Detailed balance". TENDL-2008 is taken from ENDF library [5].

As shown in Fig. 10, all the measured cross sections are significantly fluctuating, which means that the resonance may play an important role for this reaction channel in this energy region. Although the present results seem to be lower than those measured by Ashergy [17], this may also be caused by the resonance and their difference is smaller than the amplitude of the fluctuation of Ashergy [17]. Since the energy region of Ashergy and that of the present measurement are not overlapped, there may not be an experimental discrepancy. Furthermore, the results of TENDL-2008 and the calculation using TALYS-1.8 code (with default input parameter) are different from the present measurement both in magnitude and in tendency.

IV. CONCLUSIONS

In the present work, cross sections of the ^{25}Mg$(n,\alpha)^{22}$Ne and the ^{25}Mg$(n,\alpha_0)^{22}$Ne reactions were measured at five neutron energy points in the 4.0–6.0 MeV region. The present results are helpful to constrain the excitation functions of the ^{25}Mg$(n,\alpha)^{22}$Ne and the ^{25}Mg$(n,\alpha_0)^{22}$Ne reactions, and so that they are useful in the content evaluation of the ^{22}Ne in meteoroids. According to the detailed balance principle, the present results can also provide some information about the ^{22}Ne$(\alpha,n)^{25}$Mg reaction, which is one of the main neutron sources for the astrophysical *s* process. In addition, the present results are different from all existing evaluations and the TALYS-1.8 calculations both in magnitude and in tendency, which indicates that further measurements and improved evaluations are demanded.

ACKNOWLEDGMENTS

The authors are indebted to the operation crew of the 4.5 MV Van de Graff accelerator of Peking University. The present work is financially supported by the National Natural Science Foundation of China (Grants No. 11475007 and No. 11775006), Science and Technology on Nuclear Data Laboratory and China Nuclear Data Center.

[1] R. C. Reedy, C. F. Herzog, and E. K. Jessberger, Earth Planet. Sci. Lett. **44**, 341 (1979).
[2] B. Lavielle, H. Sauvageon, and P. Bertin, Phys. Rev. C **42**, 305 (1990).
[3] Live Chart of Nuclides, https://www-nds.iaea.org/relnsd/vcharthtml/VChartHTML.html.
[4] EXFOR: Experimental Nuclear Reaction Data, https://www-nds.iaea.org/exfor/exfor.htm.
[5] ENDF: Evaluated Nuclear Data File, https://www-nds.iaea.org/exfor/endf.htm.
[6] X. Zhang, Z. Chen, Y. Chen *et al.*, Phys. Rev. C **61**, 054607 (2000).
[7] G. Zhang, J. Chen, G. Tang *et al.*, J. Isotopes **18**, 29 (2005).
[8] H. Bai, H. Jiang, Z. Cui *et al.*, Determination of the amount of ^{238}U target nuclei and simulation of the neutron induced fission fragment energy spectrum, Appl. Radiat. Isot., ARI_2018_92_R1 (unpublished).
[9] H. Bai, Z. Wang, L. Zhang *et al.*, Appl. Radiat. Isot. **125**, 34 (2017).
[10] G. Zhang, H. Wu, J. Zhang *et al.*, Eur. Phys. J. A **43**, 1 (2010).
[11] C. Ji, D. Huang, T. Wang *et al.*, J. Isotopes **28**, 93 (2015).
[12] A. Koning, S. Hilaire, and S. Goriely, User Manual of talys-1.8 (Nuclear Research and Consultancy Group, Petten, 2015).
[13] J. F. Ziegler, SRIM -2013, http://www.srim.org/#SRIM.
[14] Neutron Cross-section Standards, 2006, https://www-nds.iaea.org/standards/Data/standards-238U_xs-data.txt.
[15] ENDF/B-VII.1: U.S. Evaluated Nuclear Data Library (2011), https://www-nds.iaea.org/exfor/endf.htm.
[16] E. Birgersson, A. Oberstedt, S. Oberstedt *et al.*, Nucl. Phys. A **817**, 1 (2009).
[17] D. Ashergy, Nucl. Phys. A **136**, 481 (1969).
[18] K. Wolke, V. Harms, H.W. Becker *et al.*, Z. Phys. A – Atomic Nuclei **334**, 491 (1989).
[19] F. Yang, Y. Wang, and F. Lu, *Nuclear Physics*, 2th ed. (Fudan University Press, China, 2002).